Ultrasound-assisted ionic-liquid extraction of hawthorn pectins: Structural features, rheological behavior, and preliminary gel-like behavior

Hao Zhang, Huiyao Zhang, Jiachen Li, Yugui Wang, Christophe Blecker, Hongbing Fan, Chuanhe Zhu

PII: S0141-8130(26)02619-X

DOI: https://doi.org/10.1016/j.ijbiomac.2026.152692

Reference: BIOMAC 152692

To appear in: *International Journal of Biological Macromolecules*

Received date: 8 April 2026

Revised date: 13 May 2026

Accepted date: 23 May 2026

Please cite this article as: H. Zhang, H. Zhang, J. Li, et al., Ultrasound-assisted ionic-liquid extraction of hawthorn pectins: Structural features, rheological behavior, and preliminary gel-like behavior, *International Journal of Biological Macromolecules* (2024), https://doi.org/10.1016/j.ijbiomac.2026.152692

Ultrasound-Assisted Ionic-Liquid Extraction of Hawthorn Pectins: Structural Features, Rheological Behavior, and Preliminary Gel-Like Behavior

Hao Zhang[a, b], Huiyao Zhang[a], Jiachen Li[d,e], Yugui Wang[c], Christophe Blecker*[b](✉), Hongbing Fan *[c](✉), Chuanhe Zhu*[a] (✉)

[a]College of Food Science and Engineering, Shandong Agricultural University, Taian 271018, China

[b]Department of Food Science and Formulation, Gembloux Agro-Bio Tech, University of Liège, Gembloux, 5030 Belgium

[c]Department of Animal and Food Sciences, University of Kentucky, Lexington, Kentucky, 40546, United States

[d]University College Cork, Cork, T12 K8AF, Ireland

[e]School of Food and Health, Beijing Technology and Business University, Beijing, 100080, China

Co-corresponding author (✉): Hongbing Fan (Hongbing.Fan@uky.edu)

Co-corresponding author (✉): Christophe Blecker (christophe.blecker@uliege.be)

Corresponding author (✉): Chuanhe Zhu (chhzhu@sdau.edu.cn & Czh293@uky.edu)

Tel/Fax:86-538-8242412; ORCID: 0000-0003-2496-3453

Abstract:

Ultrasound-assisted extraction (UAE) combined with ionic liquids (ILs) has been increasingly applied for pectin recovery by promoting cell-wall disintegration and polysaccharide release under mild conditions. However, limited information is available on the structural and network-related characteristics of hawthorn pectin fractions obtained under different ultrasound-assisted ionic-liquid extraction windows. In this study, hawthorn pectins were extracted using ultrasound-assisted extraction (UAE) with four ionic liquids: [Bmim]Cl, [Emim][Ac], [Amim]Cl, and [Bmim][HSO_4], with aqueous UAE used as the control. All samples were homogalacturonan-dominated low-methoxyl pectins (galacturonic acid (GalA) ≥ 74.1%, degree of esterification (DE) ≤ 43.0%). Specifically, the [Amim]Cl-extracted pectin achieved the highest yield (7.93%), whereas BH-HP showed the highest weight-average molecular weight (Mw, 856.36 kDa) and peak temperature (274.16 °C). In contrast, [Emim][Ac] yielded pectin with the lowest DE (25.03%) and smallest hydrodynamic size. All samples showed pronounced shear-thinning behavior, but differed in viscoelastic balance and temperature responsiveness, indicating distinct aggregation and network-related characteristics after redispersion in water. In addition, the CK-HP/[Bmim][HSO_4] system showed concentration-dependent spectral and rheological changes along with inversion-resistant gel-like behavior, suggesting preliminary gel-like network formation in this ionic-liquid medium. These findings indicate that IL-specific optimized UAE extraction windows generated hawthorn pectin fractions with distinct structural and colloidal/network-related behaviors, providing a basis for application-oriented formulation design.

Keywords: Hawthorn pectin; Ionic liquids; Rheological properties

1. Introduction

Hawthorn residues, a major by-product of fruit storage and processing, contain nearly 10% pectin, yet these residues remain largely underutilized [1,2]. Hawthorn pectin, owing to its high GalA content, may exhibit favorable gelling, stabilizing, emulsifying, and thickening properties compared with some commercial citrus or apple pectins. This indicates potential for its use as a functional polysaccharide in model colloidal and material-related systems[3-6]. The functional performances of hawthorn pectin, including gelation strength, thermal stability, and interfacial activity, are critically controlled by its molecular architecture (DE, GalA content, neutral sugar composition, and Mw distribution), which is highly dependent on the extraction technology [7-10]. However, conventional hot-acid, alkali, or aqueous extraction often has drawbacks such as high energy consumption and pectin degradation [11,12], highlighting the need for alternative and more selective extraction strategies that preserve or tailor desirable pectin structural features.

Ionic liquids (ILs), consisting of organic cations and inorganic or organic anions, have attracted considerable attention as alternative solvents because of their negligible vapor pressure, adjustable solvating ability, high thermal stability, and unique ability to disrupt hydrogen-bonding networks in carbohydrate assemblies [13,14]. Dialkylimidazolium-based ionic liquids exhibit relatively acidic C2–H protons (pKa ≈20~23), which render the C2–H proton relatively labile and may enhance hydrogen-bonding interactions [15,16]. When paired with strongly hydrogen-bond-accepting anions (e.g., Cl^-, Ac^-), these ILs can effectively

disrupt the intramolecular and intermolecular hydrogen-bonding networks in cellulose and other wall polysaccharides [17-19]. This disruptive process enhances the dissolution of cell wall components, thereby promoting the release of pectin. In pectin extraction, IL-containing systems have been reported to improve extraction efficiency and modify physicochemical properties, although the resulting structural changes depend strongly on solvent composition and processing conditions [20-23]. Furthermore, several studies have demonstrated that combining UAE with ILs can offer synergistic benefits by accelerating solvent penetration, intensifying cavitation effects, reducing extraction time and energy consumption, while maintaining pectin structural integrity [24-27].

Although ultrasound-assisted extraction combined with ionic liquids has been reported for polysaccharide and pectin recovery, limited information is available on how different imidazolium-based IL extraction windows affect the structural descriptors and network-related behavior of hawthorn pectin. In particular, hawthorn pectin remains less studied than citrus and apple pectins in IL-assisted extraction systems, despite its high GalA content, HG-dominated composition, and promising thickening and gel-related properties. The present work therefore compares hawthorn pectin fractions obtained under IL-specific optimized UAE conditions using four imidazolium-based ILs, namely [Bmim]Cl, [Emim][Ac], [Amim]Cl, and [Bmim][HSO_4], with aqueous UAE as the control. The resulting fractions were characterized in terms of extraction performance, chemical composition, molecular descriptors, thermal behavior, microstructure, and rheological properties. In addition, the behavior of CK-HP was preliminarily examined in a [Bmim][HSO_4]-containing medium to evaluate its gel-like response. By combining extraction metrics, residue-marker

screening, molecular descriptors, aqueous rheology, preliminary gel-like behavior, and scenario-based ranking, this study provides an application-oriented comparison of UAE–IL-derived hawthorn pectin fractions. Because each solvent was evaluated under its own optimized extraction window, the comparison should not be interpreted as a strict single-factor test of IL identity under identical extraction conditions.

2. Materials and methods

2.1 Materials and reagents

Hawthorn residues were provided by the College of Food Science and Engineering, Shandong Agricultural University (Tai'an, China), and stored at 4 ℃ until use. The ionic liquids [Bmim]Cl (≥97% purity), [Emim][Ac] (≥99% purity), [Amim]Cl (≥96% purity), and [Bmim][HSO_4] (≥95% purity) were purchased from Shanghai Macklin Biochemical Technology Co., Ltd. All chemical reagents were of analytical grade.

2.2 Ultrasound-assisted ionic liquid and aqueous extraction of hawthorn pectin

Hawthorn residues were pulverized and passed through a 50-mesh sieve. Aqueous IL solutions were prepared by dissolving the required amount of each IL in deionized water to the target molarity and stirring until complete dissolution. The pH of the extraction media was not externally adjusted. The initial apparent pH values of the aqueous extraction media were measured at 25 ℃ after complete dissolution of each IL and before addition of hawthorn powder using a calibrated pH meter. Each extraction medium was independently prepared and measured in triplicate. The measured values are provided in Supplementary Table S3. The powders were mixed with IL solutions at a solid-to-solvent ratio of 1:10 (w/v), and extraction was performed using a bath-type ultrasonic device (KQ-1000DE, Kunshan Ultrasonic

Instruments Co., Ltd., Kunshan, China) at a set ultrasonic power of 360 W. These conditions were selected from preliminary orthogonal screening to maximize pectin extraction for each IL system [28]. Because the temperature, time, and IL concentration were optimized separately for each solvent, the resulting fractions should be interpreted as products obtained under IL-specific optimized UAE windows, rather than as samples generated under a strict single-factor design for isolating IL identity. The optimized ultrasonic conditions for each ionic liquid were as follows (guided by Jiang and Kou) [23,29]: (i) [Bmim]Cl: 60 min, 60 ℃, 1 mol/L; (ii) [Bmim][HSO_4]: 60 min, 60 ℃, 0.6 mol/L; (iii) [Emim][Ac]: 50 min, 80 ℃, 0.6 mol/L; (iv) [Amim]Cl: 60 min, 70 ℃, 0.6 mol/L.

After extraction, the mixtures were centrifuged at 4500 rpm for 15 min. The supernatant was concentrated to one-third of its initial volume under reduced pressure in a rotary evaporator, mixed with 95% (v/v) ethanol to obtain a final ethanol concentration of 70%, and stored at 4 ℃ for 24 h to induce precipitation. The precipitate was redissolved in deionized water and reprecipitated once under the same ethanol conditions. The precipitate was collected by filtration and washed three times with 95% (v/v) ethanol (each time redispersed in ethanol, mixed for 10 minutes, and then filtered again) [30]. The extraction yield reported in Table 2 refers to the mass of freeze-dried purified pectin obtained after precipitation, reprecipitation, ethanol washing, and freeze-drying, relative to the initial dry hawthorn powder. Stepwise recovery yields during purification were not independently recorded and therefore are not reported. The precipitate was collected and freeze-dried to obtain ionic-liquid-extracted hawthorn pectin fractions (BCl-HP, BH-HP, EAc-HP and ACl-HP). Ultrasound-assisted aqueous extraction followed the same workflow, using deionized water

instead of ionic liquids, with a solid-to-solvent ratio of 1:10 (w/v), ultrasonic power of 360 W, extraction time of 60 min, and extraction temperature of 60 ℃. Subsequent processing steps were identical, yielding the control hawthorn pectin (CK-HP).

Energy consumption was estimated based on the set ultrasonic power and the recorded operating time: Energy consumption (kWh)= power (kW) × processing time (h). Lab-scale process specific energy was calculated as energy (kWh) per kg of recovered pectin (kg), with the pectin mass normalized to that obtained from 1 kg of dry hawthorn powder [31,32].

2.3 Determination of basic physicochemical properties

2.3.1 Hawthorn pectin yield

The calculation formula of hawthorn pectin yield (Y) was:

$$Y\ (\%) = \frac{M}{M_1} \times 100\% \quad (1)$$

where M is the mass of recovered hawthorn pectin (g), and M_1 is the mass of dry hawthorn powder (g).

2.3.2 GalA content measurement

The GalA content of hawthorn pectin samples was determined using the m-hydroxybiphenyl method [33]. A standard curve (y = 0.6093x + 0.0157) was constructed using a galacturonic acid standard solution (0.1 mg/mL). Briefly, 1 mL of hawthorn pectin solution (0.1 mg/mL) was added to 5 mL of borax–sulfuric acid reagent under ice-bath conditions and mixed thoroughly. The mixture was then heated in a water bath at 80 ℃ for 6 min, cooled to room temperature, and supplemented with 0.1 mL of 0.15% (w/v) m-hydroxybiphenyl solution. After shaking, the reaction mixture was allowed to stand at 25 ℃ for 20 min. The absorbance was recorded at 520 nm, and the GalA content was calculated

from the standard curve.

2.3.3 Degree of esterification (DE)

The degree of esterification (DE) of hawthorn pectin was determined using an acid–base titration method following Bu et al. [34], with phenolphthalein as the indicator. Briefly, 0.5% (w/v) pectin solution was prepared, and phenolphthalein was added. The sample was titrated with 0.1 mol/L NaOH to the endpoint (a faint pink color persisting for 30 s), and the consumed volume was recorded as V_1 (mL). Subsequently, 2 mL of 0.5 mol/L NaOH was added, the mixture was shaken thoroughly, and allowed to stand at room temperature for 20 min to saponify methyl esters. The excess alkali was then back-titrated with 0.5 mol/L HCl until the pink color just disappeared. After adding 4–6 drops of phenolphthalein again, the solution was titrated with 0.1 mol/L NaOH to the same endpoint, and the consumed volume was recorded as V_2 (mL). The DE was calculated as:

$$DE\ (\%) = \frac{V_2}{A_1 + A_2} \times 100\% \quad (2)$$

where V_1 corresponds to neutralization of free carboxyl groups and V_2 corresponds to carboxyl groups released after saponification of esterified groups.

2.3.4 Protein content

The protein content of hawthorn pectin was determined by the Bradford method with BSA as the standard [35].

2.3.5 Hydrodynamic size and ζ-potential

Hawthorn pectin was dissolved in deionized water to prepare 2 mg/mL solution, and the hydrodynamic size was measured at room temperature using a Zeta potential analyzer (Zeta Plus, Brookhaven, USA). The hawthorn pectin solution was adjusted to pH 7.0 by 0.1 mol/L

NaOH solution. The samples were then transferred to cuvettes and analyzed for ζ-potential.

2.3.6 Monosaccharide composition and HG/RG-I estimation

The hawthorn pectin solution was hydrolyzed with trifluoroacetic acid (TFA) in a boiling water bath for 3 h. After cooling, the hydrolysate was centrifuged to collect the supernatant. A 1 mL aliquot of the supernatant was mixed with 0.3 mL of aqueous ammonia and sodium borohydride and maintained at 40 ℃ for 1 h. The reaction was quenched by adding 0.4 mL of glacial acetic acid. For derivatization, 1 mL of the resulting solution was combined with 0.5 mL of 1-methylimidazole and 4.5 mL of acetic anhydride. After 10 min, the reaction was terminated by adding 10 mL of deionized water, followed by cooling in an ice bath. The derivatives were extracted two to three times with dichloromethane, and the combined organic phase was adjusted to 10 mL with dichloromethane. The extract was filtered through a 0.45 μm membrane, and 2.0 μL of the filtrate was injected at 250 ℃ for gas chromatographic (GC) analysis. Neutral monosaccharides were separated on a DM-2330 capillary column (30 m × 0.32 mm × 0.2 μm) with nitrogen as the carrier gas [1]. The standard monosaccharides included rhamnose (Rha), arabinose (Ara), xylose (Xyl), mannose (Man), galactose (Gal) and glucose (Glu).

The relative proportions of homogalacturonan (HG) and rhamnogalacturonan-I (RG-I) regions were estimated from the measured contents of GalA (%) and Rha (%) according to the following equation:

$$\text{HG}\ (\%) = \frac{\frac{G}{194} - \frac{R}{164}}{\frac{G}{194}} \times 100\% \tag{3}$$

$$\text{RG-I}\ (\%) = \frac{\frac{\text{R}}{164}}{\frac{\text{G}}{194}} \times 100\% \quad (4)$$

where the G denotes the GalA content (%), and R denotes the Rha content (%). This calculation provides an approximate domain-level descriptor and should not be interpreted as direct linkage-level structural determination.

2.3.7 Molecular weight distribution

The molecular weight distribution was determined using high-performance gel permeation chromatography (HPGPC) reported by Sun et al. with minor modifications [7]. Freeze-dried hawthorn pectin was dissolved in 0.1 mol/L $NaNO_3$ to obtain a 2.0 mg/mL solution, then filtered through a 0.22 μm membrane prior to injection. HPGPC analysis was conducted on a system equipped with a size-exclusion column and a refractive index detector. The mobile phase was 0.1 mol/L $NaNO_3$ at 0.6 mL/min, with a column temperature of 30 ℃ and a 20 μL injection. Calibration was performed using 2 mg/mL of P-82 pullulan.

2.4 Determination of residual counter-anion markers in pectin fractions

Residual counter-anions were quantified as targeted markers to assess potential carryover from the corresponding ionic-liquid media (chloride for chloride-based ionic liquids, acetate for acetate-based ionic liquids, and sulfate species reported as SO_4^{2-} equivalents for $[HSO_4]^-$-based ionic liquids). Chloride was determined by an argentometric back-titration (Volhard method; GB 5009.44-2016; aligned with ASTM D512). Sulfate species were quantified by the $BaSO_4$ turbidimetric method (GB/T 5750.5-2023; ASTM D516). Acetate was quantified using a commercial enzyme-coupled acetate assay kit according to the manufacturer's protocol. Method reporting limits in assay solutions were: Cl^- <8 mg/L;

sulfate (as SO_4^{2-} equivalents) <5 mg/L; acetate (as Ac^-) <4.5 mg/L (Table 2). Imidazolium cation residues were not quantified in the present study. Therefore, the residue analysis should be interpreted as targeted counter-anion screening rather than a complete ionic-liquid residue or food-grade safety assessment.

2.5 Fourier transform infrared spectroscopy (FT-IR) analysis

The hawthorn pectin sample was tested by Fourier-transform infrared spectrometer (Nexus 670, Thermo Fisher Scientific, USA). The test conditions were set as follows: the resolution was 2 cm^{-1}, 64 scans were performed. The absorption spectrum was collected in the frequency range of 4000-400 cm^{-1} and the infrared spectrum was obtained after correction.

2.6 Raman spectroscopy analysis

Raman spectra were recorded by DXR2xi Raman imaging microscope (Thermo, USA) equipped with a 50× objective (NA = 0.8) using a 785 nm laser source. Spectra of the hawthorn pectin sample (3200–400 cm^{-1}) were collected at three randomly selected locations with 0.5 s exposure time and 5.0 mW laser power [36].

2.7 Morphological analysis by scanning electron microscopy (SEM)

The freeze-dried hawthorn pectin sample was fixed on the sample stage using conductive adhesive and sputter-coated with gold. The surface morphology of the hawthorn pectin was observed by scanning electron microscopy (Inspect F50, FEI, USA) at different magnifications (150×, 500×, 1k×, 2k×, 5k×), with an accelerating voltage set at 2 kV [37].

2.8 X-ray diffraction (XRD)

The crystal structure of the hawthorn pectin sample was characterized using an X-ray diffraction (Bruker D8 Advance, Germany). Cu-Kα radiation was used to scan the diffraction

angle (2θ) of the hawthorn pectin sample in sections over a scanning range of 5°-60° at a rate of 2°/min. The current and voltage during the test were 40 mA and 40 kV, respectively [38].

2.9 Thermal Analysis

The thermal properties of the hawthorn pectin samples were analyzed using a TG-DSC thermal analyzer (NETZSCH, STA449F3 Jupiter, Germany). 2 mg sample of hawthorn pectin was placed in an alumina crucible and heated in a range of 30–600℃ at heating rate of 10℃/min under nitrogen atmosphere [39].

2.10 Dynamic rheological measurements of aqueous pectin solutions

The hawthorn pectin solution was prepared in deionized water to 2% (w/v) and stirred for 4 hours at 25℃ to ensure uniform mixing. The rheological properties of the sample were measured using a modular intelligent rheometer (AR2000ex, TA Instruments, USA) equipped with 20 mm and 50 mm parallel plates [40].

2.10.1 Steady shear viscosity

The hawthorn pectin solution was placed on parallel plates (20 mm) and equilibrated at 25℃ for 5 minutes. Steady-state shear was used to measure the apparent viscosity at shear rates ranging from 0.1 to 100 s^{-1}.

2.10.2 Frequency sweep

Dynamic oscillatory sweep tests were used to determine the loss moduli (G") and storage moduli (G') of hawthorn pectin samples. The viscoelastic properties of the samples were quantified under the following experimental conditions: angular frequency (0.1-100 rad/s), temperature (25℃), and oscillatory strain (0.1%).

2.10.3 Temperature sweep

Dynamic temperature oscillatory sweep tests were used to determine the trends in the loss moduli (G") and storage moduli (G') of hawthorn pectin samples at different temperatures. The samples were placed on parallel plates (50 mm) and the temperature range was set at 25-90℃ (5℃/min) with an angular frequency of 1 rad/s.

2.11 Preparation of pectin–ionic liquid dispersions for preliminary gel-like behavior assessment

CK-HP was dispersed in aqueous IL media (1.0 mol/L) to preliminarily assess concentration-dependent gel-like behavior in ionic-liquid-containing systems [41]. CK-HP powder was added gradually under continuous stirring until homogeneous dispersions were obtained, and pectin concentrations were adjusted to 1.0%, 1.5%, 2.0%, 2.5%, and 3.0% (w/v). The dispersions were degassed and allowed to equilibrate at room temperature without disturbance. Gel-like behavior in the IL-containing medium was preliminarily assessed using a vial inversion test after equilibration.

2.12 FT-IR and Raman analysis of CK-HP/[Bmim][HSO_4] gel-like systems

FT-IR and Raman spectra were collected using the same instrumental configurations and data-processing procedures described in Sections 2.5 and 2.6, respectively. Samples were measured as dispersions or equilibrated gel-like systems according to their physical state, with handling minimized and samples kept sealed to reduce moisture uptake of the ionic liquid.

2.13 Rheological measurements of CK-HP/[Bmim][HSO_4] gel-like systems

The viscoelastic properties of CK-HP/[Bmim][HSO_4] dispersions and gel-like systems were measured using a rotational rheometer following the protocol described for aqueous pectin systems (Section 2.10). Measurements were performed with a parallel-plate geometry

equipped with anti-slip surfaces and a solvent trap to limit moisture exchange. Strain-amplitude sweeps were conducted to determine the linear viscoelastic region, followed by frequency sweeps to obtain G′ and G″; steady shear viscosity was recorded over a controlled shear-rate range at the same controlled temperature.

2.14 Comparative evaluation of hawthorn pectin fractions

An analytic hierarchy process–technique for order preference by similarity to ideal solution (AHP–TOPSIS) framework was used to compare the five hawthorn pectin fractions under scenario-specific decision settings [42,43]. The five experimentally obtained fractions, CK-HP, BCl-HP, BH-HP, EAc-HP, and ACl-HP, were defined as the alternatives. The quantitative descriptors reported in Tables 2 and 3 were used as the evaluation criteria. FT-IR, Raman, SEM, and XRD results were used only for structural interpretation and were not included as TOPSIS criteria.

Three decision scenarios were constructed. Scenario 1 represented process efficiency and included extraction yield and lab-scale process specific energy. Scenario 2 represented network-forming material potential and included weight-average molecular weight (Mw), GalA content, ζ-potential magnitude, degree of esterification (DE), and hydrodynamic size. Scenario 3 represented model colloid structuring potential and included bound protein content, ζ-potential magnitude, RG-I proportion, DE, and hydrodynamic size. The target direction and AHP-derived weights used in each scenario are summarized in Table 1. The three scenarios were treated as independent TOPSIS exercises; therefore, closeness coefficients and rankings were interpreted only within each scenario and were not compared or aggregated across scenarios. The pairwise comparison matrices, AHP-derived weights, and consistency

parameters are provided in Supplementary Tables S1a–S1d. Pairwise judgments followed Saaty's reciprocal comparison scale, where 1 indicates equal importance and larger values indicate stronger relative importance of the row criterion over the column criterion. "Higher preferred" indicates that a larger value was considered more desirable within the corresponding scenario, whereas "Lower preferred" indicates that a smaller value was considered more desirable. The absolute value of ζ-potential was used because the magnitude of surface charge was considered in the descriptor-based comparison.

For each scenario, an AHP pairwise comparison matrix was constructed only among the selected criteria, not among the alternatives. The matrix was expressed as:

$$A = (a_{jk})_{n \times n} \tag{6}$$

Where a_{jk} represents the relative importance of criterion j over criterion k, and n is the number of criteria in the corresponding scenario. The normalized priority vector obtained from the matrix was used as the AHP weight vector:

$$w = (w_1, w_2, \dots, w_n)^T \tag{7}$$

Thus, the number of AHP weights corresponded exactly to the number of criteria included in each scenario. The resulting criterion weights were then used in the TOPSIS calculation.

The initial decision matrix was defined as:

$$X = (x_{ij})_{m \times n} \tag{8}$$

Where x_{ij} is the observed value of alternative i under criterion j, m is the number of alternatives, and n is the number of criteria. The decision matrix was normalized as follows:

$$r_{ij} = \frac{x_{ij}}{\sqrt{\sum_{i=1}^{m} x_{ij}^2}} \tag{9}$$

The weighted normalized matrix was calculated as:

$$v_{ij} = w_j r_{ij} \tag{10}$$

Where w_j is the AHP-derived weight of criterion j.

For criteria with a "Higher preferred" target, the positive ideal solution was defined as the maximum value and the negative ideal solution as the minimum value. For criteria with a "Lower preferred" target, the positive ideal solution was defined as the minimum value and the negative ideal solution as the maximum value. The distances of each alternative to the positive and negative ideal solutions were then calculated as:

$$D_i^+ = \sqrt{\sum_{j=1}^{n} (v_{ij} - A_j^+)^2} \quad D_i^- = \sqrt{\sum_{j=1}^{n} (v_{ij} - A_j^-)^2} \tag{11}$$

The closeness coefficient was then calculated as:

$$C_i = \frac{D_i^-}{D_i^+ + D_i^-} \tag{12}$$

A larger C_i value indicates that the alternative is closer to the positive ideal solution and farther from the negative ideal solution. The alternatives were ranked in descending order of C_i.

To evaluate ranking stability, a one-at-a-time sensitivity analysis was performed by increasing or decreasing each criterion weight by 20%, followed by proportional renormalization of the remaining weights. The TOPSIS ranking was recalculated under each perturbed-weight condition. The complete sensitivity-analysis results are provided in Supplementary Table S2.

Table 1. Criteria, target direction, and AHP-derived weights used for independent scenario-specific TOPSIS ranking

Scenario	Criterion	Target	Weight
Scenario 1	Yield	Higher preferred	0.500

Scenario 1	Specific energy	Lower preferred	0.500
Scenario 2	Mw	Higher preferred	0.310
Scenario 2	GalA	Higher preferred	0.058
Scenario 2	|ζ-potential|	Higher preferred	0.161
Scenario 2	DE	Lower preferred	0.310
Scenario 2	Size	Lower preferred	0.161
Scenario 3	Protein	Higher preferred	0.326
Scenario 3	|ζ-potential|	Higher preferred	0.180
Scenario 3	RG-I	Higher preferred	0.061
Scenario 3	DE	Lower preferred	0.326
Scenario 3	Size	Lower preferred	0.107

Note: CK-HP, BCl-HP, BH-HP, EAc-HP, and ACl-HP were treated as alternatives. The three scenarios were calculated as independent TOPSIS exercises, and rankings should be interpreted only within each scenario. "Higher preferred" and "Lower preferred" indicate the target direction assigned to each criterion under the corresponding scenario. The AHP pairwise comparison matrices, derived weights, and consistency parameters are provided in Supplementary Tables S1a–S1d.

2.15 Statistical analysis

Statistical analyses were performed using SPSS Statistics 26.0. Unless otherwise stated, data are expressed as mean ± standard deviation (n=3). Here, n=3 denotes three independent extractions, and each reported value represents the mean of analytical measurements on these independent extracts. One-way analysis of variance followed by Tukey's post hoc test ($P < 0.05$) was applied to compare the five resulting pectin fractions (CK-HP, BCl-HP, BH-HP, EAc-HP, and ACl-HP) for the quantitative endpoints reported in the tables and figures. Significant differences are indicated by different superscript letters. Because extraction parameters were optimized separately for each ionic liquid, these statistical comparisons describe differences among the resulting fractions under IL-specific optimized UAE windows rather than the isolated effect of ionic-liquid identity under identical processing conditions. They should not be interpreted as a strict single-factor test of IL identity under identical temperature, time, and concentration.

3. Results and discussion

3.1 Yield, energy metrics and physicochemical properties of hawthorn pectins

3.1.1 Extraction yield, lab-scale process specific energy, and residual counter-anion markers

Table 2. Yield, lab-scale process specific energy, and residual counter-anion markers of hawthorn pectins

	CK-HP	BCl-HP	BH-HP	EAc-HP	ACl-HP
Yield (%)	5.85±0.13^{c}	6.77±0.29^{b}	5.68±0.26^{c}	6.36±0.23^{b}	7.93±0.31^{a}
Cl^-	-	ND	-	-	ND
SO_4^{2-} equivalents	-	-	ND	-	-
Ac^-	-	-	-	ND	-
Energy consumption (kWh)	0.36	0.36	0.36	0.3	0.36
Specific energy (kWh/kg)	6.15 ±0.14^{a}	5.32 ±0.23^{b}	6.34 ±0.29^{a}	4.72 ±0.17^{c}	4.54 ±0.18^{c}

ND: not detected below the method reporting limits in assay solutions: Cl^- < 8 mg/L; sulfate, reported as SO_4^{2-} equivalents, < 5 mg/L; acetate, as Ac^-, < 4.5 mg/L. "–": not applicable. These results refer only to targeted counter-anion screening and do not represent complete ionic-liquid residue analysis. Because imidazolium cation residues were not quantified, these data should not be used to support food-grade safety or complete IL-removal claims. Values are means ± standard deviation (n = 3). Different letters within the same row indicate significant differences ($P < 0.05$).

Extraction yield and lab-scale process energy metrics were evaluated under the laboratory protocol. As shown in Table 2, ACl-HP showed the highest extraction yield (7.93%), followed by BCl-HP and EAc-HP. BH-HP was statistically comparable to the aqueous UAE control, indicating that not all IL-containing systems improved pectin recovery under their respective optimized conditions. Because extraction conditions were optimized separately for each IL, these differences reflect the combined effects of the IL environment and its optimized processing window, rather than the isolated effect of IL identity [13]. Process electricity use per batch was similar across routes (0.30–0.36 kWh), and the lab-scale process specific energy therefore mainly reflected differences in recovered pectin mass: ACl-HP and EAc-HP

exhibited lower specific energy (≈4.5–4.7 kWh/kg), whereas BH-HP showed higher values. This trend is consistent with the view that ionic-liquid physicochemical properties and solvent–biopolymer interactions can affect dissolution efficiency and process energy intensity in biomass processing [18]. The residual counter-anion markers, including Cl^-, Ac^-, and sulfate species reported as SO_4^{2-} equivalents, were not detected above the method reporting limits in the purified hawthorn pectin fractions. This result suggests low counter-anion carryover after ethanol precipitation and washing. However, because imidazolium cation residues were not quantified, complete removal of ionic-liquid residues cannot be confirmed from the present data, and no food-grade safety conclusion should be drawn from this screening alone.

3.1.2 Degree of esterification and bound protein

The five hawthorn pectin samples (Table 3) exhibited moderate to low degrees of esterification (DE range: 25.03–42.92%), classifying them as low-methoxyl pectins (LM pectins, DE < 50%). The relatively low DE is indicative of a greater proportion of free carboxyl groups ($–COO^-$) available for electrostatic interactions with proteins and cations in food matrices [44]. EAc-HP showed the lowest DE, suggesting that the [Emim][Ac]-based UAE system was associated with greater de-esterification of hawthorn pectin under the present extraction conditions [45]. The protein contents of the different hawthorn pectins were low, ranging from 1.84 to 2.19% (Table 3). No significant differences were observed among CK-HP, BCl-HP, BH-HP and ACl-HP ($p > 0.05$), whereas EAc-HP showed a slightly higher protein level (2.19%), as indicated by its distinct superscript. Moderate levels of protein have been demonstrated to enhance emulsifying properties, while excessive protein incorporation

may interfere with the formation of stable gel networks [46].

Table 3. Physicochemical and molecular characteristics of hawthorn pectins obtained by different UAE－IL systems

	CK-HP	BCl-HP	BH-HP	EAc-HP	ACl-HP
DE (%)	42.92±0.24^{a}	36.41±0.13^{b}	36.57±0.19^{b}	25.03±0.31^{d}	35.44±0.18^{c}
Monosaccharide composition					
GalA (%)	86.97±0.05^{a}	78.03±0.12^{d}	83.18±0.17^{c}	83.96±0.19^{b}	74.17±0.09^{e}
Rha (%)	0.89±0.02^{a}	0.81±0.01^{b}	0.74±0.03^{c}	0.75±0.01^{c}	0.81±0.02^{b}
Ara (%)	1.13±0.04^{a}	0.86±0.03^{b}	0.70±0.02^{c}	0.86±0.03^{b}	0.69±0.02^{c}
Xyl (%)	3.24±0.12^{a}	0.96±0.07^{c}	1.16±0.09^{b}	0.96±0.06^{c}	0.97±0.08^{c}
Man (%)	0.54±0.05^{b}	0.64±0.06^{a}	0.40±0.04^{b}	0.44±0.01^{b}	0.48±0.04^{b}
Gal (%)	2.30±0.02^{b}	2.03±0.06^{c}	2.56±0.04^{a}	1.65±0.03^{d}	1.98±0.01^{c}
Glc (%)	2.94±0.16^{a}	2.71±0.11^{a}	2.76±0.14^{a}	1.71±0.13^{c}	2.08±0.12^{b}
HG (%)	98.79±0.03^{a}	97.47±0.02^{c}	97.98±0.04^{b}	97.98±0.01^{b}	97.19±0.02^{c}
RG-I (%)	1.21±0.01^{d}	2.5±0.02^{b}	2.02±0.04^{c}	2.01±0.01^{c}	2.81±0.02^{a}
Molecular weight					
Mw (kDa)	430.07±0.72^{e}	674.72±0.24^{b}	856.36±0.56^{a}	479.78±0.48^{d}	575.58±0.61^{c}
Mn (kDa)	204.69±0.86^{c}	228.89±0.27^{b}	404.97±0.19^{a}	158.23±0.23^{e}	198.24±0.34^{d}
Mw/Mn	2.11±0.13^{b}	2.95±0.24^{a}	2.09±0.16^{b}	3.03±0.46^{a}	2.90±0.15^{a}
Protein content (%)	1.84±0.05^{b}	1.87±0.08^{b}	1.89±0.07^{b}	2.19±0.12^{a}	1.95±0.02^{b}
Size (nm)	639.53±16.05^{a}	294.54±22.17^{b}	263.2±2.65^{c}	138.43±1.49^{d}	252.2±3.9^{b}
ζ-potential (mV)	-10.67±0.31^{c}	-8.39±0.33^{e}	-16.37±0.45^{a}	-9.35±0.41^{d}	-13.27±0.38^{b}

Note: Values are expressed as means ± standard deviation (n = 3). Different superscript letters within the same row indicate significant differences ($P < 0.05$).

3.1.3 Monosaccharide composition and HG/RG-I domains

In all samples (Table 3), CK-HP exhibited the highest GalA content (86.97%) and the lowest estimated RG-I proportion (1.21%), whereas ACl-HP showed the highest estimated RG-I proportion. BH-HP retained relatively high GalA content (83.18%) with a moderate estimated RG-I value (2.02%), while EAc-HP showed a comparable GalA level and a relatively balanced HG/RG-I profile. These results indicate that the different extraction

windows recovered hawthorn pectin fractions with different monosaccharide compositions and estimated domain tendencies [47]. Because the HG/RG-I values were calculated from monosaccharide composition, they should be interpreted as compositional descriptors rather than direct evidence of linkage pattern or detailed side-chain architecture [48].

3.1.4 Molecular weight and polydispersity

As shown in Table 3, BH-HP exhibited the highest Mw (856.36 kDa), suggesting that the [Bmim][HSO_4]-based UAE window favored the recovery of a higher-Mw pectin under the present conditions [49]. CK-HP showed a comparatively lower Mw, which may be related to the stronger mechanical effects of aqueous ultrasonic extraction on chain disentanglement and partial depolymerization [22]. EAc-HP presented a moderate Mw (479.78 kDa) but the largest Mw/Mn value (3.03), indicating a broader molecular-weight distribution. This broader distribution suggests that the [Emim][Ac]-based extraction window recovered pectin populations with more heterogeneous chain sizes, rather than a narrowly distributed polymer fraction [46,50]. The chloride-containing systems, BCl-HP and ACl-HP, produced intermediate-to-high Mw fractions accompanied by relatively high Mw/Mn values, indicating that these fractions also contained molecular populations with wider chain-size distributions [51]. Overall, the Mw and Mw/Mn results show that the different UAE–IL extraction windows produced hawthorn pectin fractions with distinct molecular-size profiles. These differences may be associated with the combined effects of solvent environment, ultrasound-assisted mass transfer, and extraction temperature/time on pectin release and chain association during extraction.

3.1.5 Hydrodynamic size and ζ-potential

The hydrodynamic size and ζ-potential results after redispersion under identical aqueous conditions indicate differences in the supramolecular association and colloidal behavior of hawthorn pectin (Table 3). CK-HP exhibited the largest hydrodynamic size (639.53 nm), whereas the IL-extracted fractions showed markedly smaller sizes. BCl-HP, ACl-HP, and BH-HP formed particles of approximately 250–290 nm, while EAc-HP showed the smallest hydrodynamic size (138.43 nm). These smaller sizes suggest a lower extent of intermolecular association and a more dispersed state in water, which is consistent with the ability of ultrasound-assisted extraction and IL-containing media to alter cell-wall polymer associations during processing [52]. The ζ-potential values also differed among the fractions. BH-HP showed the most negative ζ-potential, followed by ACl-HP, CK-HP, EAc-HP, and BCl-HP. The more negative value of BH-HP may be related to its lower DE and a higher apparent density of ionized carboxyl groups after redispersion in water [53]. However, the ζ-potential trend did not strictly follow DE alone, indicating that surface charge behavior was also affected by molecular-size distribution and supramolecular association. Taken together, the differences in hydrodynamic size and ζ-potential suggest that the IL-specific extraction windows generated fractions with different dispersion states and charge-related colloidal behavior. These changes may be related to differences in solvent acidity/basicity, hydrogen-bonding capacity, and ionic environment among the tested IL systems [54].

3.2 Spectroscopic and morphological signatures of hawthorn pectins extracted by different ionic liquids

3.2.1 FT-IR and Raman spectral characteristics

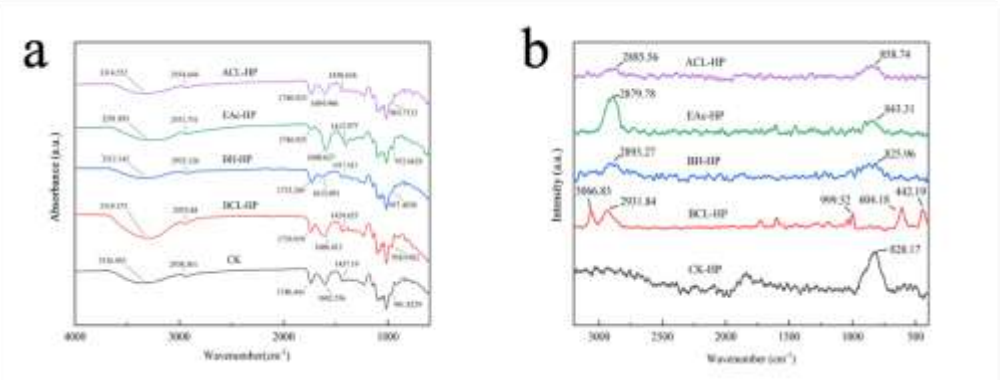

Fig. 1. FT-IR (a) and Raman (b) spectra of hawthorn pectins obtained using different UAE–IL extraction systems

The FT-IR spectra of hawthorn pectins showed clear differences among fractions obtained using different extraction media (Fig. 1a). The broad O–H stretching vibration band at 3200–3400 cm^{-1} and the C–H stretching vibration band at 2920–2940 cm^{-1} confirm the abundant presence of hydroxyl and methylene groups [55]. Among the samples, BCl-HP exhibited the broadest O–H stretching band, CK-HP showed intermediate intensity, whereas EAc-HP and BH-HP displayed weaker signals. The characteristic absorption band at 1740 cm^{-1} corresponds to the C=O stretching vibration of methyl esterified galacturonic acid, while the absorption band at 1600–1630 cm^{-1} is attributed to the asymmetric $–COO^-$ stretching vibration. These characteristic absorption bands are commonly used to assess esterification-related differences in pectin [56]. Compared to the control group (CK-HP), the esterification degree of hawthorn pectin extracted with ionic liquids exhibited varying degrees of reduction, with EAc-HP displaying the lowest esterification level. Symmetrical carboxylate stretching is observable at 1400–1450 cm^{-1}, with an occasional weak shoulder peak (ester C–O) at 1240 cm^{-1}. The fingerprint region (1200–800 cm^{-1}) remains distinctly preserved across all samples (particularly at ≈1015, ≈970, and <920 cm^{-1}), suggesting that the main polysaccharide fingerprint features were retained despite differences in DE [57-59]. Raman

spectra (Fig. 1b) were employed to reveal C–H stretching bands at 2880–2930 cm^{-1} across all samples, alongside hawthorn pectin sugar ring vibrations near 820–860 cm^{-1} and 1000 cm^{-1}, and backbone vibrations of α-(1→4) glycosidic bonds in the main chain [60,61]. In comparison with CK-HP, which displays a solitary main peak at 820 cm^{-1}, ACl-HP, BH-HP, and EAc-HP exhibit distinct peaks at 858 cm^{-1}, 826 cm^{-1}, and 843 cm^{-1}, respectively, reflecting differences in GalA esterification and ionic state. BCl-HP did not show a clear peak in this region, likely due to overlapping signals from mixed esterification states [46].

3.2.2 Macroscopic appearance and SEM microstructure

As shown in Fig. 2, hawthorn pectin extracted using different ionic liquids exhibited distinct color and morphological features, reflecting differences in dried-state appearance and morphology among the fractions [62,63]. The macroscopic color changed from a uniform light creamy-white (CK-HP) to a light reddish-brown (EAc-HP and BH-HP), while BCl-HP and ACl-HP displayed lighter beige-brown tones. These color differences may be associated with differences in co-extracted minor components or extraction-induced changes in dried-state appearance, although these components were not quantified in the present study. SEM analysis revealed that all freeze-dried hawthorn pectin samples exhibited a porous dried matrix, yet substantial variations were evident in terms of pore size and wall morphology. CK-HP exhibited large and irregular pores with locally collapsed edges, whereas BCl-HP presented thicker struts and more ordered lamellar features. BH-HP, which had the highest Mw, displayed a visibly dense and compact network with small, tightly connected pores, suggesting that a densified dried-state matrix was favored under [Bmim][HSO_4] conditions. In contrast, EAc-HP and ACl-HP showed more porous structures with smoother pore walls and

more rounded cavities, indicating a looser reorganization of polysaccharide chains during drying. The extraction environment under each IL-specific optimized window may influence DE and molecular-weight distribution, thereby contributing to differences in dried-state network morphology [52,64].

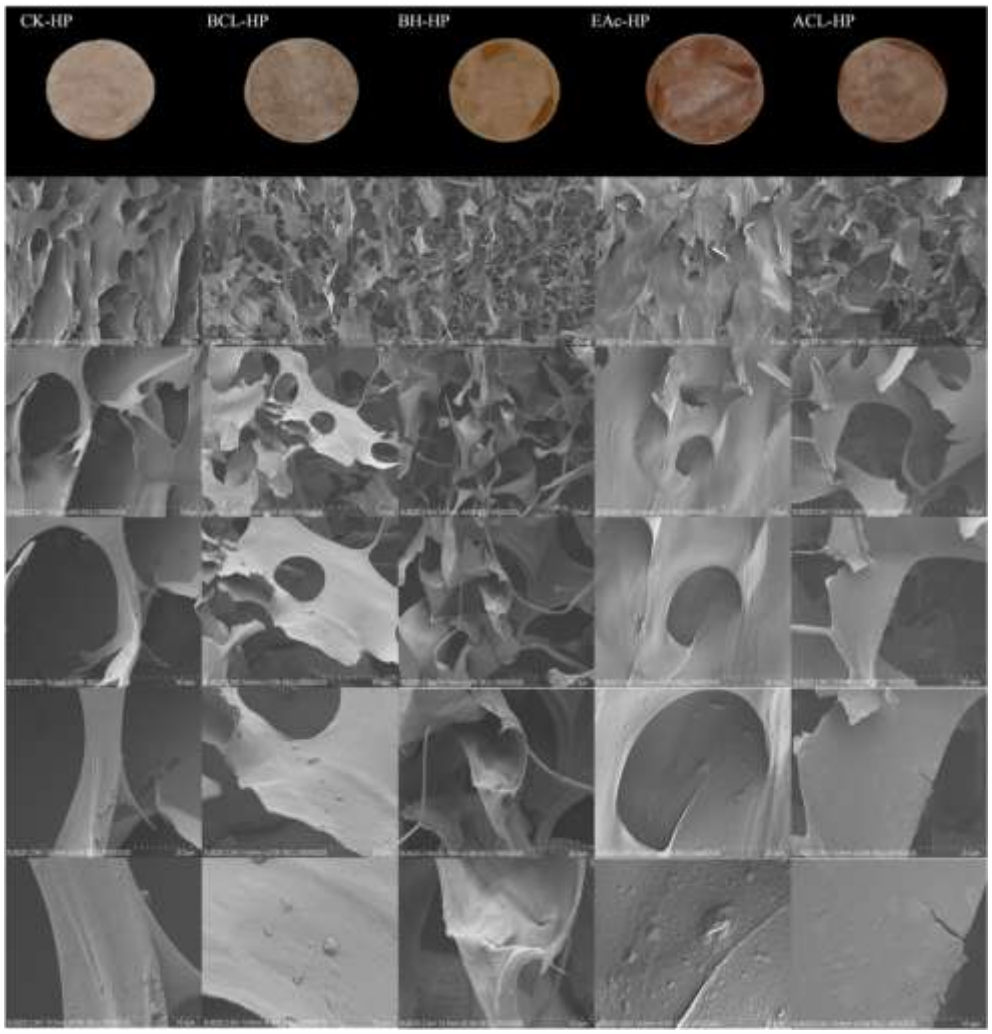

Fig. 2. Macroscopic appearance and SEM microstructure of hawthorn pectins obtained using different UAE–IL extraction systems

3.2.3 XRD patterns

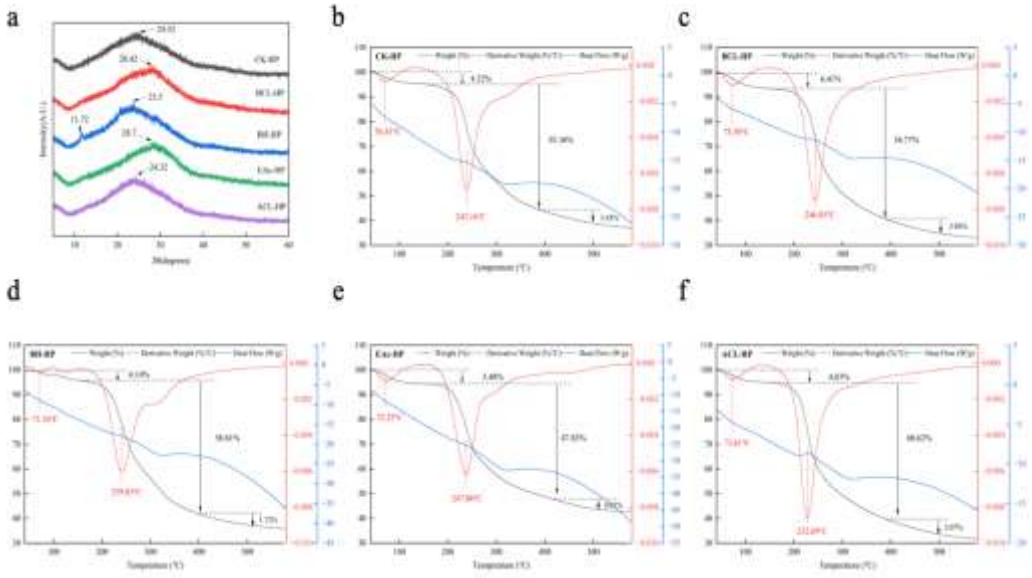

Fig. 3. XRD patterns (a) and thermal degradation behavior (b–f) of hawthorn pectins extracted by different UAE－IL systems

Five hawthorn pectin samples (Fig. 3a) exhibited a typical amorphous halo, with diffraction peaks located between 20° and 30° at 2θ, indicating predominantly amorphous structures with short-range ordered domains [65]. The diffraction peaks of BCl-HP and EAc-HP shifted upward to 28.4° and 28.7° at 2θ, respectively, suggesting a decrease in the average interlayer spacing or tighter short-range packing [66]. The diffraction peak of BH-HP exhibited a shift towards the lower angle (2θ) of 23.5°, accompanied by the emergence of a weak shoulder at approximately 11.7°. The lower peak position may indicate changes in short-range packing and higher structural disorder. Although BH-HP showed a compact freeze-dried morphology in SEM, its XRD profile suggested lower short-range ordering. This indicates that SEM morphology and XRD chain-packing features reflect different structural scales [67]. The diffraction peaks of ACl-HP and CK-HP were both around 24.3°. However, the ACl-HP peak was broader, indicating a higher degree of amorphous structure.

3.3 Thermal stability of hawthorn pectins

As illustrated in Fig. 3b-f, the thermal degradation behaviors of the five hawthorn pectin

samples exhibit three distinct stages of mass loss with increasing temperature. The first stage corresponds to the evaporation of free and bound water from the pectin matrix [68], with mass losses of 4–6% (CK 4.52%, BCl 6.41%, BH 4.14%, EAc 5.48%, ACl 4.83%). The second stage, characterized by a sharp decrease in mass, is mainly associated with the thermal decomposition of the polysaccharide backbone and cleavage of glycosidic linkages [69]. The order of weight loss was ACl-HP > BH-HP > BCl-HP > CK-HP > EAc-HP, indicating that the ACl-HP sample was the least thermally stable. At higher temperatures, the third stage corresponds to carbonization, where the degradation rate decreases progressively. The residual masses at the end of the process followed the sequence EAc-HP (42.69%) > CK-HP (36.87%) > BH-HP (35.52%) > BCl-HP (32.94%) > ACl-HP (31.48%). The DSC thermograms revealed peak temperatures of 243.16, 246.85, 274.16, 248.86, and 232.69 ℃ for CK-HP, BCl-HP, BH-HP, EAc-HP, and ACl-HP, respectively, during the second degradation stage. The thermal profiles therefore indicated sample-dependent stability depending on the parameter considered. ACl-HP showed the largest mass loss during the main degradation stage, suggesting lower resistance to thermal mass loss. BH-HP exhibited the highest peak temperature in the main degradation region, indicating delayed maximum degradation under the tested conditions. EAc-HP retained the highest residual mass at 600 °C, suggesting greater char residue formation. These differences indicate that thermal behavior was not governed by a single structural descriptor, but was associated with molecular-weight distribution, esterification degree, monosaccharide composition, and intermolecular association generated under the different UAE–IL extraction windows.

3.4 Rheological analysis of hawthorn pectin

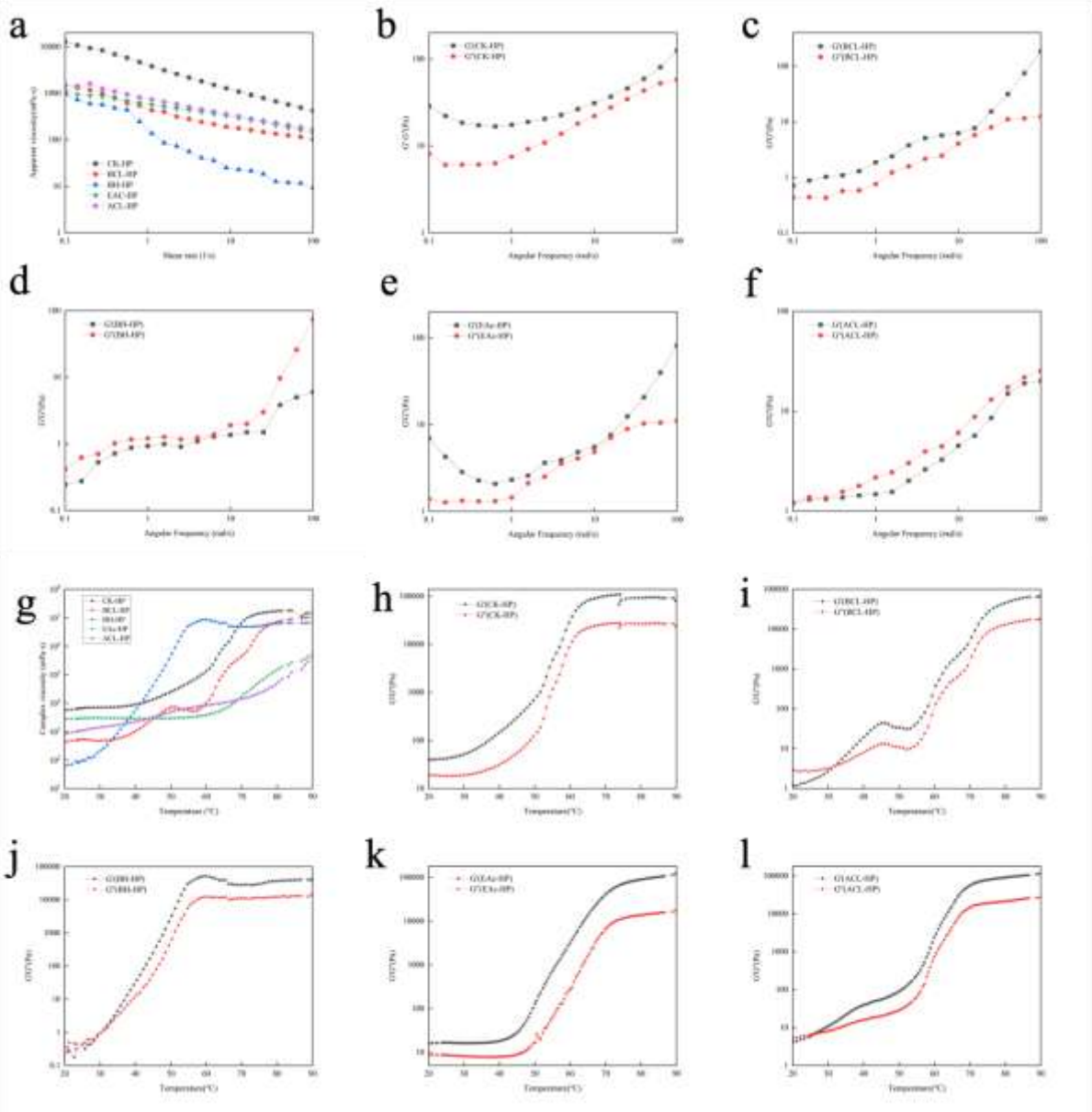

Fig. 4. Steady shear viscosity (a), frequency sweeps of storage and loss moduli (b–f), complex viscosity (g) and temperature sweeps (h–l) of aqueous hawthorn pectin solutions

As shown in Fig. 4a, all samples displayed significant shear-thinning behavior. At low shear rates, the apparent viscosity followed the order: CK-HP > BCl-HP ≈ ACl-HP ≈ EAc-HP > BH-HP. At higher shear rates, pectin chains were progressively oriented along the flow direction, leading to reduced apparent viscosity. Although CK-HP had the lowest Mw, its relatively higher DE, less negative ζ-potential, and larger hydrodynamic size (Table 3) suggest reduced electrostatic repulsion and enhanced intermolecular aggregation in water, which may

account for its higher apparent viscosity at low shear rates. In contrast, BH-HP had the highest Mw but showed the lowest apparent viscosity under the tested aqueous conditions. This indicates that viscosity was not governed by Mw alone, but also by molecular-size distribution, charge density, hydrodynamic association, and chain aggregation state under the tested aqueous conditions.

Frequency sweep tests (Fig. 4b–f) showed that both G′ and G″ increased monotonically with angular frequency. CK-HP, EAc-HP, and BCl-HP consistently exhibited G′ > G″, indicating a predominantly elastic response, whereas BH-HP and ACl-HP exhibited weaker viscoelastic profiles, with viscous dissipation contributing more prominently [30]. One possible explanation is that, under identical aqueous conditions, fractions with higher DE contain fewer ionized carboxyl groups, which can reduce electrostatic repulsion and facilitate transient intermolecular association [70]. Temperature sweeps (Fig. 4h–l) showed temperature-dependent increases in both G′ and G″ for all samples, especially within approximately 50–80 °C. CK-HP and EAc-HP maintained G′ higher than G″ throughout the measured temperature range, indicating an elastic-dominated response under the selected conditions. In contrast, BCl-HP, BH-HP, and ACl-HP showed changes in the relative magnitude of the two moduli at the low-temperature stage. For BCl-HP and BH-HP, G′ became higher than G″ after approximately 30 °C, whereas ACl-HP showed this change after approximately 25–30 °C. The complex viscosity curves (Fig. 4g) also increased during heating, supporting thermally induced thickening with sample-dependent differences in onset temperature and magnitude [71].

3.5 Preliminary gel-like behavior of CK-HP in [Bmim][HSO_4]-containing medium

3.5.1 Macroscopic gel-like behavior in aqueous IL systems

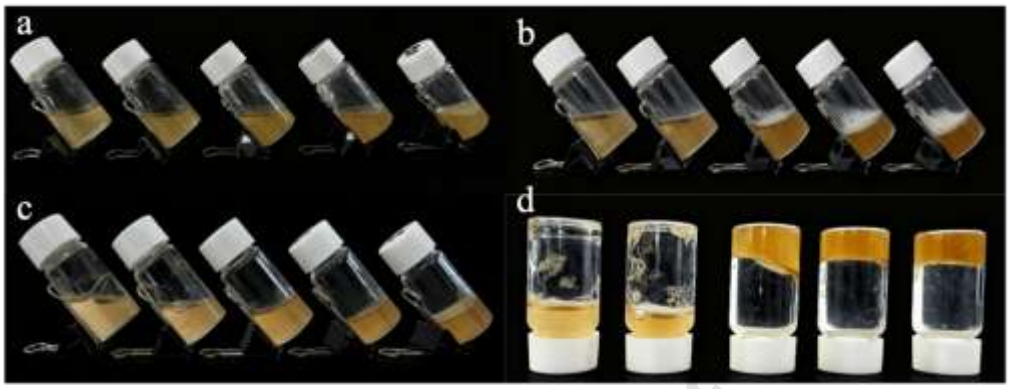

Fig. 5. Macroscopic appearance of CK-HP at different concentrations in aqueous IL systems

The vial inversion tests (Fig. 5) showed that CK-HP dispersions prepared in 1 mol/L [Bmim]Cl, [Amim]Cl, and [Emim][Ac] remained flowable across the tested concentration range, although viscosity increased gradually with concentration. In contrast, the CK-HP/[Bmim][HSO_4] system displayed a clear transition toward inversion-resistant, self-supporting gel-like behavior at pectin concentrations of ≥ 2.0% (w/v). Under the present aqueous ionic-liquid conditions, this result suggests that the [Bmim][HSO_4]-containing medium was associated with stronger macroscopic gel-like behavior than the other tested media [72]. However, this observation should be interpreted as preliminary evidence of gel-like behavior in an ionic-liquid-containing medium rather than definitive proof of a fully characterized ionogel material.

3.5.2 FT-IR and Raman characterization of CK-HP/[Bmim][HSO_4] gel-like systems

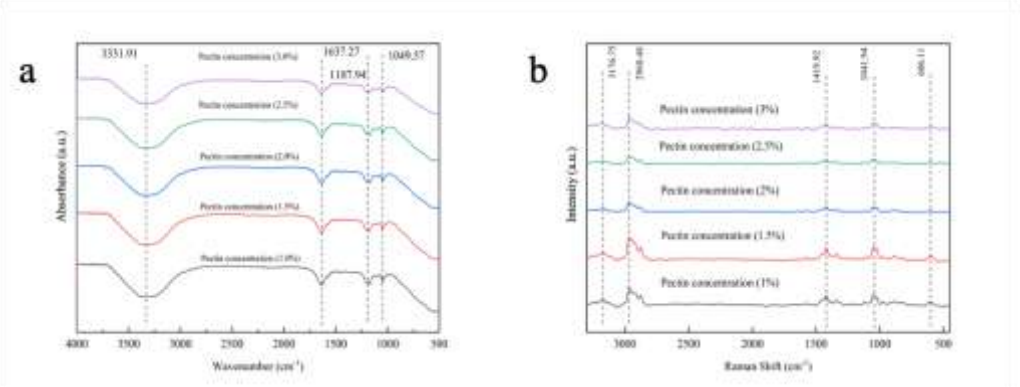

Fig. 6. FT-IR (a) and Raman (b) spectra of CK-HP/[Bmim][HSO_4] dispersions at different hawthorn pectin concentrations

The FT-IR and Raman results support concentration-dependent interactions in the CK-HP/[Bmim][HSO_4] system. With increasing pectin concentration, the absence of new major characteristic bands suggests that the main polysaccharide backbone remained chemically intact, whereas the slight broadening and shift of the O–H band indicate strengthened non-covalent interactions within the medium [73,74]. These spectral changes are consistent with enhanced hydrogen bonding and altered ionic microenvironments as the system evolved from a dispersion toward a more highly associated gel-like state [75]. In the Raman spectra, changes associated with the imidazolium- and sulfate-related signals further support concentration-dependent interactions between hawthorn pectin and the ionic-liquid medium [76].

3.5.3 Rheological properties of CK-HP/[Bmim][HSO_4] gel-like systems

The rheological results were in agreement with the macroscopic observations. Increasing CK-HP concentration in [Bmim][HSO_4] led to a marked increase in apparent viscosity and progressively higher G′ and G″ values, with G′ remaining above G″ over the measured frequency range. This trend is consistent with the progressive development of a more highly associated, network-like viscoelastic structure in the ionic-liquid-containing medium. At 2.5–

3.0% (w/v), the weak frequency dependence of G′ and the elevated modulus values indicated the development of a more highly associated, solid-like viscoelastic response in the [Bmim][HSO_4]-containing medium [77]. Nevertheless, additional measurements, such as gel strength, solvent-retention capacity, long-term stability, and microscopic network observation, are required before this system can be fully defined as an ionogel material.

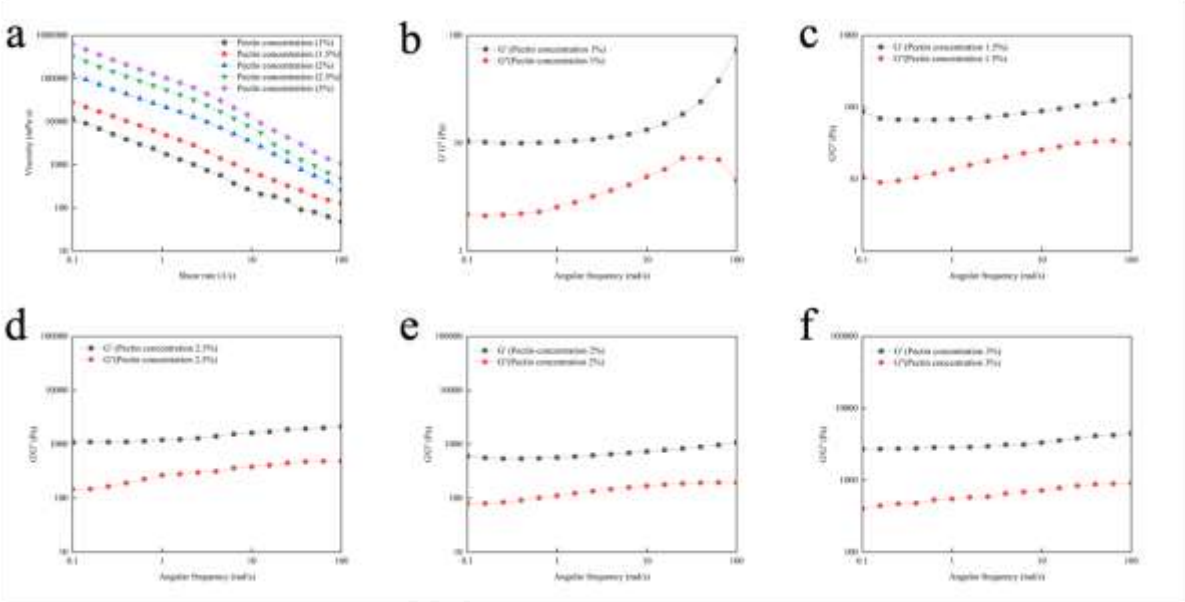

Fig. 7. Steady shear viscosity (a) and frequency sweeps of storage and loss moduli (b–f) of CK-HP/[Bmim][HSO_4] gel-like systems at different hawthorn pectin concentrations

3.6 Comparative evaluation of hawthorn pectin fractions

The AHP–TOPSIS analysis was used to provide a scenario-specific comparison of the measured quantitative descriptors, rather than to identify a universally superior hawthorn pectin fraction. In this analysis, CK-HP, BCl-HP, BH-HP, EAc-HP, and ACl-HP were treated as alternatives, while the selected process-related and physicochemical parameters were treated as criteria.

The target direction of each criterion was assigned according to the intended use of the ranking scenario. In Scenario 1, higher yield and lower specific energy were considered

favorable for process efficiency. In Scenario 2, higher Mw, higher GalA content, and larger ζ-potential magnitude were considered favorable for network-forming material potential, whereas lower DE and smaller hydrodynamic size were preferred because they indicate more available carboxyl groups and better redispersion under the tested aqueous conditions. In Scenario 3, bound protein content, ζ-potential magnitude, and RG-I proportion were treated as favorable descriptors for colloid structuring, whereas DE and hydrodynamic size were assigned a “Lower preferred” target.

The TOPSIS results are shown in Table 4. Under Scenario 1, ACl-HP ranked first because it combined the highest extraction yield with relatively low lab-scale process specific energy. EAc-HP ranked second, mainly due to its low specific energy. BH-HP ranked last because its yield was comparable to the aqueous control, while its specific energy was relatively high.

Under Scenario 2, BH-HP showed the highest closeness coefficient, mainly because of its high Mw and larger ζ-potential magnitude. EAc-HP ranked second, which was associated with its low DE and small hydrodynamic size. CK-HP ranked last in this scenario, mainly due to its large hydrodynamic size and less favorable weighted distance from the positive ideal solution.

Under Scenario 3, EAc-HP ranked first because of its low DE, small hydrodynamic size, and relatively high bound protein content. BH-HP and ACl-HP ranked second and third, respectively, indicating that these fractions also showed favorable colloid-structuring-related descriptors but did not present the same overall balance as EAc-HP under this weighting scheme.

Table 4. TOPSIS distances, closeness coefficients, and rankings of hawthorn pectin fractions under three decision scenarios

	Alternative	D^+	D^-	C	Rank
	ACl-HP	0	0.1063	1	1
	EAc-HP	0.054	0.0702	0.5655	2
Scenario 1	BCl-HP	0.0508	0.0559	0.5238	3
	CK-HP	0.0967	0.0097	0.0911	4
	BH-HP	0.1063	0	0	5
	BH-HP	0.0513	0.1327	0.7213	1
	EAc-HP	0.094	0.1226	0.5659	2
Scenario 2	ACl-HP	0.0802	0.0936	0.5384	3
	BCl-HP	0.0829	0.0915	0.5246	4
	CK-HP	0.1583	0.0143	0.0828	5
	EAc-HP	0.0482	0.1029	0.6808	1
	BH-HP	0.0556	0.0785	0.5853	2
Scenario 3	ACl-HP	0.0528	0.0715	0.5752	3
	BCl-HP	0.0778	0.0554	0.4158	4
	CK-HP	0.1109	0.0153	0.1214	5

Note: D^+ and D^- represent the distances to the positive and negative ideal solutions, respectively. C is the TOPSIS closeness coefficient. Alternatives were ranked in descending order of C within each scenario. Because the three scenarios were calculated independently using different criteria and weights, C values should not be compared across scenarios.

The sensitivity analysis showed that the top-ranked fraction in each scenario remained unchanged after ±20% one-at-a-time weight perturbation (Table 5). This suggests that the main top-rank outcomes were stable within the present decision framework. However, some intermediate alternatives changed position under perturbed-weight conditions, indicating that the ranking still depended on the selected criteria and assigned weights. Therefore, the AHP–TOPSIS results should be regarded as a descriptor-based decision-support analysis rather than a direct functional-performance test. The rankings provide a transparent way to compare measured descriptors within predefined application scenarios, but they require validation in target formulation or material systems after appropriate residue and safety assessment.

Table 5. Stability of AHP–TOPSIS rankings under ±20% criterion-weight perturbation

	Top-ranked alternative	Sensitivity summary
Scenario 1	ACl-HP	The top rank remained unchanged in all tests
Scenario 2	BH-HP	The top rank remained unchanged; rank exchanges occurred only among intermediate alternatives
Scenario 3	EAc-HP	The top rank remained unchanged; minor exchanges occurred among intermediate alternatives

Note: In each sensitivity test, one criterion weight was increased or decreased by 20%, and the remaining weights were proportionally renormalized to maintain a total weight of 1. The TOPSIS ranking was recalculated after each perturbation. Complete rankings and closeness coefficients under each perturbation condition are provided in Supplementary Table S2.

4. Conclusion

Hawthorn pectin fractions obtained using different imidazolium-based UAE–IL extraction windows exhibited distinct structural and rheological profiles. Under their respective optimized extraction conditions, the fractions were compared in terms of extraction performance, structural descriptors, rheological behavior, preliminary gel-like behavior, and independent scenario-based AHP–TOPSIS evaluation. Among the fractions, ACl-HP showed the highest recovery, EAc-HP exhibited the lowest DE and the finest aqueous dispersion, whereas BH-HP presented the highest Mw and a distinct thermal–rheological profile. The independent AHP–TOPSIS analysis provided scenario-specific guidance, identifying ACl-HP as preferable for process efficiency, BH-HP for network-forming material potential, and EAc-HP for model colloid structuring potential. These rankings should be interpreted as descriptor-based guidance rather than evidence of universal functional superiority. The interpretation is also limited by the IL-specific optimized extraction windows, the counter-anion-only residue screening, and the preliminary nature of the CK-HP/[Bmim][HSO_4] gel-like assessment. Further matched-condition extraction,

imidazolium cation residue analysis, and gel-network characterization are therefore needed.

Conflicts of Interest

The authors declare no conflict of interest related to the publication of this manuscript.

Acknowledgments

This research was financially supported by Key R&D Program of Shandong Province, China (2024TZXD004, 2023TZXD030).

Author contribution

Hao Zhang: Investigation, Methodology, Data curation, Validation, Writing-original draft; Huiyao Zhang: Visualization, Data analysis; Jiachen Li: Investigation, Writing; Yugui Wang: Resources, Validation; Hongbing Fan*: Conceptualization, Supervision, Writing – review & editing; Christophe Blecker: Methodology, Supervision, Writing – review & editing; Chuanhe Zhu: Conceptualization, Project administration, Funding acquisition, Supervision, Visualization, Writing – review & editing.

References

[1] C. Qin, G. Yang, C. Zhu, M. Wei, Characterization of edible film fabricated with HG-type hawthorn pectin gained using different extraction methods, Carbohydr. Polym. 285 (2022) 119270. https://doi.org/10.1016/j.carbpol.2022.119270

[2] Z. Li, J. Zhang, H. Zhang, Y. Liu, C. Zhu, Effect of different processing methods of hawthorn on the properties and emulsification performance of hawthorn pectin, Carbohydr. Polym. 298 (2022) 120121. https://doi.org/10.1016/j.carbpol.2022.120121

[3] M. Kavya, A. Ranjit Jacob, P. Nisha, Pectin emulsions and emulgels: Bridging the correlation between rheology and microstructure, Food Hydrocoll. 143 (2023) 108868. https://doi.org/10.1016/j.foodhyd.2023.108868

[4] W.L. Liang, J.S. Liao, J.R. Qi, W.X. Jiang, X.Q. Yang, Physicochemical characteristics and functional properties of high methoxyl pectin with different degree of esterification, Food Chem. 375 (2022) 131806. https://doi.org/10.1016/j.foodchem.2021.131806

[5] L. Li, X. Gao, J. Liu, B. Chitrakar, B. Wang, Y. Wang, Hawthorn pectin: Extraction, function

and utilization, Curr. Res. Food Sci. 4 (2021) 429-435. https://doi.org/10.1016/j.crfs.2021.06.002

[6] Riyamol, J.G. Chengaiyan, S.S. Rana, F. Ahmad, S. Haque, E. Capanoglu, Recent advances in the extraction of pectin from various sources and industrial applications, ACS Omega 8 (2023) 46309-46324. https://doi.org/10.1021/acsomega.3c04010

[7] D. Sun, X. Chen, C. Zhu, Physicochemical properties and antioxidant activity of pectin from hawthorn wine pomace: A comparison of different extraction methods, Int. J. Biol. Macromol. 158 (2020) 1239-1247. https://doi.org/10.1016/j.ijbiomac.2020.05.052

[8] W. Sun, K. Bu, H. Meng, C. Zhu, Physicochemical properties of pectin-Fe(III) gained by HG-type hawthorn with different esterification degree, Int. J. Biol. Macromol. 274 (2024) 132886. https://doi.org/10.1016/j.ijbiomac.2024.132886

[9] H. Zhang, W. Sun, A. Qayum, M. Li, C. Zhu, Preparation, characterization and sustained release of an encapsulated astaxanthin composite derived from hawthorn pectin/zein hydrogel, Int. J. Biol. Macromol. 308 (2025) 142417. https://doi.org/10.1016/j.ijbiomac.2025.142417

[10] Y. Zhu, H. Wang, T. Zhang, X. Zhang, C. Zhu, Characterization, antioxidant activity and in vitro digestion of hawthorn pectin prepared by gradient ethanol precipitation, Int. J. Biol. Macromol. 267 (2024) 131278. https://doi.org/10.1016/j.ijbiomac.2024.131278

[11] X. Wang, Y. Sun, Y. Yu, D. Huang, Y. Liu, M. Huang, Y. Jiang, D. Li, Sequential extraction of hawthorn pectin: An attempt to reveal their original mode of being in plants and functional properties, Int. J. Biol. Macromol. 282 (2024) 136756. https://doi.org/10.1016/j.ijbiomac.2024.136756

[12] T. Xiang, R. Yang, L. Li, H. Lin, G. Kai, Research progress and application of pectin: A review, J. Food Sci. 89 (2024) 6985-7007. https://doi.org/10.1111/1750-3841.17438

[13] T. Uto, Atomistic simulations of polysaccharide materials for insights into their crystal structure, nanostructure, and dissolution mechanism, Polym. J. 57 (2025) 33-41. https://doi.org/10.1038/s41428-024-00966-x

[14] J. Yu, X. Liu, S. Xu, P. Shao, J. Li, Z. Chen, X. Wang, Y. Lin, C.M.G.C. Renard, Advances in green solvents for production of polysaccharide-based packaging films: Insights of ionic liquids and deep eutectic solvents, Compr. Rev. Food Sci. Food Saf. 22 (2023) 1030-1057. https://doi.org/10.1111/1541-4337.13099

[15] S. Neyrizi, J. Kiewiet, M.A. Hempenius, G. Mul, What it takes for imidazolium cations to promote electrochemical reduction of CO2, ACS Energy Lett. 7 (2022) 3439-3446. https://doi.org/10.1021/acsenergylett.2c01372

[16] S. Sowmiah, V. Srinivasadesikan, M.C. Tseng, Y.H. Chu, On the chemical stabilities of ionic liquids, Molecules 14 (2009) 3780-3813. https://doi.org/10.3390/molecules14093780

[17] S. Taokaew, Recent advances in cellulose-based hydrogels prepared by ionic liquid-based processes, Gels 9 (2023) 546. https://doi.org/10.3390/gels9070546

[18] R. Cao, H. Gao, W. Lv, Y. Song, Y. Long, B. Ren, Y. Nie, S.J. Zhang, Nanoscale insights into cellulose–imidazolium ionic liquid interactions via atomic force microscopy,

Carbohydr. Polym. 380 (2026) 125073. https://doi.org/10.1016/j.carbpol.2026.125073

[19] T. Endo, K. Hamada, M. Kawahara, R. Kihara, H. Sugihara, Y. Kimura, Dissolution of cellulose in imidazolium carboxylate with long alkyl chain, Bull. Chem. Soc. Jpn. 99 (2026) 10. https://doi.org/10.1093/bulcsj/uoag010

[20] M.A. Wan Chik, R. Yusof, M.H. Shafie, R. Mohamed Hanaphi, The versatility of pectin: a comprehensive review unveiling its recovery techniques and applications in innovative food products, J. Food Meas. Charact. 18 (2024) 6101-6123. https://doi.org/10.1007/s11694-024-02632-5

[21] E.S. Morais, A.M.C. Lopes, M.G. Freire, C.S.R. Freire, J.A.P. Coutinho, A.J.D. Silvestre, Use of ionic liquids and deep eutectic solvents in polysaccharides dissolution and extraction processes towards sustainable biomass valorization, Molecules 25 (2020) 3652. https://doi.org/10.3390/molecules25163652

[22] Z. Liu, L. Qiao, H. Gu, F. Yang, L. Yang, Development of Brönsted acidic ionic liquid based microwave assisted method for simultaneous extraction of pectin and naringin from pomelo peels, Sep. Purif. Technol. 172 (2017) 326-337. https://doi.org/10.1016/j.seppur.2016.08.026

[23] S.Q. Jiang, Y.G. Chai, S.F. Ma, J.F. Wang, W.P. Shi, P.P. He, J.X. Pang, Y.G. Lin, Ultrasound-assisted ionic liquid extraction of polysaccharides from Crataegus Songarica K. Koch fruits: Structural characterization and antioxidant activity, Chem. Biodivers. 22 (2025) e202402386. https://doi.org/10.1002/cbdv.202402386

[24] M. Wang, C. Li, J. Li, W. Hu, A. Yu, H. Tang, J. Li, H. Kuang, H. Zhang, Extraction, purification, structural characteristics, biological activity and application of polysaccharides from Portulaca oleracea L. (Purslane): A Review, Molecules 28 (2023) 4813. https://doi.org/10.3390/molecules28124813

[25] P. Karbuz, N. Tugrul, Microwave and ultrasound assisted extraction of pectin from various fruits peel, J. Food Sci. Technol. 58 (2021) 641-650. https://doi.org/10.1007/s13197-020-04578-0

[26] P. Lasunon, N. Sengkhamparn, Effect of ultrasound-assisted, microwave-assisted and ultrasound-microwave-assisted extraction on pectin extraction from industrial tomato waste, Molecules 27 (2022) 1157. https://doi.org/10.3390/molecules27041157

[27] Y. Wu, S. Yao, B.A. Narale, A. Shanmugam, S. Mettu, M. Ashokkumar, Ultrasonic processing of food waste to generate value-added products, Foods 11 (2022) 2035. https://doi.org/10.3390/foods11142035

[28] M. Imran, C.H. Weng, G.S. Wolde, Y.C. Chen, Y.J. Wu, S.M. Huang, Y.T. Lin, Ultrasound-assisted deep eutectic solvent-based extraction of polysaccharides from okra: Optimization by response surface methodology and artificial neural network modeling, Ultrason. Sonochem. 124 (2026) 107715. https://doi.org/10.1016/j.ultsonch.2025.107715

[29] X. Kou, Y. Ke, X. Wang, M.R.T. Rahman, Y. Xie, S. Chen, H. Wang, Simultaneous extraction of hydrophobic and hydrophilic bioactive compounds from ginger (Zingiber officinale Roscoe), Food Chem. 257 (2018) 223-229. https://doi.org/10.1016/j.foodchem.2018.02.125

[30] W. Wang, P.Y. Nakasu, J.M. Costa, F. D'Acierno, N. Ahmad, M.M. Titirici, D. Pontiroli, M.

Riccò, C. Hu, J.P. Hallett, Pectin Extracted by a Recyclable Molecular Mixture: A Promising Material for Porous Membranes in Quasi-Solid-State Na-Ion Batteries, ACS Sustainable Chem. Eng. 13 (2025) 18061-18074. https://doi.org/10.1021/acssuschemeng.5c07306

[31] E. Bouloumpasi, A. Skendi, S. Christaki, C.G. Biliaderis, M. Irakli, Optimizing conditions for the recovery of lignans from sesame cake using three green extraction methods: Microwave-, ultrasound- and accelerated-assisted solvent extraction, Ind. Crops Prod. 207 (2024) 117770. https://doi.org/10.1016/j.indcrop.2023.117770

[32] J. Li, G. Ye, Z. Zhou, J. Wang, J. Wang, T. Ju, A. Cifuentes, E. Ibañez, D. Baranenko, H. Zhao, W. Lu, Ultrasound-assisted extraction of polysaccharide from Allium chinense G. Don epidermal waste: Evaluation of extraction mechanism, physicochemical properties, and bioactivities, Ultrason. Sonochem. 112 (2025) 107210. https://doi.org/10.1016/j.ultsonch.2024.107210

[33] E. Şen, E. Göktürk, V. Hajiyev, E. Uğuzdoğan, Comparisons of pulsed ultrasound-assisted and hot-acid extraction methods for pectin extraction under dual acid mixtures from onion (Allium cepa L.) waste, Food Sci. Nutr. 11 (2023) 7320-7329. https://doi.org/10.1002/fsn3.3657

[34] K. Bu, S. Wu, C. Zhu, M. Wei, Comparative study of HG-type low-ester hawthorn pectin as a promising material for the preparation of hydrogel, Carbohydr. Polym. 296 (2022) 119941. https://doi.org/10.1016/j.carbpol.2022.119941

[35] M.M. Bradford, A rapid and sensitive method for the quantitation of microgram quantities of protein utilizing the principle of protein-dye binding, Anal. Biochem. 72 (1976) 248-254. https://doi.org/10.1016/0003-2697(76)90527-3

[36] C. Chen, X. Wang, X. Wang, G.I.N. Waterhouse, M. Jiang, X. Qiao, Z. Xu, "One-Pot" readout cyano-programmable sers-encoded platform enables ultrasensitive and interference-free detection of multitarget bioamines, Anal. Chem. 96 (2024) 12862-12874. https://doi.org/10.1021/acs.analchem.4c02582

[37] V.H.A. Ribeiro, M.E.R.M. Cavalcanti-Mata, R.L.J. Almeida, V.M.A. Silva, Characterization and evaluation of heat–moisture-modified black and red rice starch: physicochemical, microstructural, and functional properties, Foods 12 (2023) 4222. https://doi.org/10.3390/foods12234222

[38] Z. Zhang, Q. Ruan, X. Sun, J. Yuan, Optimization of enzymolysis modification conditions of dietary fiber from bayberry pomace and its structural characteristics and physicochemical and functional properties, Molecules 29 (2024) 3415. https://doi.org/10.3390/molecules29143415

[39] X. Feng, Y. Wang, A. Qayum, C. Zhou, H. Fan, C. Zhu, Maillard reaction products-induced structural and functional enhancement of rice flour gels for dysphagia-oriented hydrocolloids, Food Res. Int. 221 (2025) 117349. https://doi.org/10.1016/j.foodres.2025.117349

[40] M.E. Karga, M.E. Kargaki, H. Iatrou, C. Tsitsilianis, pH-Responsive, thermo-resistant poly(acrylic acid)-g-poly(boc-l-lysine) hydrogel with shear-induced injectability, Gels 8 (2022) 817. https://doi.org/10.3390/gels8120817

[41] A. Takada, J. Kadokawa, Fabrication and characterization of polysaccharide ion gels with ionic liquids and their further conversion into value-added sustainable materials, Biomolecules 5 (2015) 244–262. https://doi.org/10.3390/biom5010244

[42] M. Behzadian, S. Khanmohammadi Otaghsara, M. Yazdani, J. Ignatius, A state-of-the-art survey of TOPSIS applications, Expert Syst. Appl. 39 (2012) 13051–13069. https://doi.org/10.1016/j.eswa.2012.05.056

[43] J. Shi, J. Yu, L. Wang, Y. Xue, C. Xue, A strategic study of multi-criteria decision-making: Functional properties and application prospects of five plant protein alternatives to animal-based products, Food Chem. 484 (2025) 144344. https://doi.org/10.1016/j.foodchem.2025.144344

[44] N.S. Said, I.F. Olawuyi, W.Y. Lee, Pectin hydrogels: Gel-forming behaviors, mechanisms, and food applications, Gels 9 (2023) 732. https://doi.org/10.3390/gels9090732

[45] P. Pękala, M. Szymańska-Chargot, A. Zdunek, Acetylated hemicelluloses and esterified pectin alterations in apple cell walls during the development of two apple cultivars: Insights from FT-IR, Raman spectroscopy, and imaging, Food Chem. 493 (2025) 146129. https://doi.org/10.1016/j.foodchem.2025.146129

[46] C.R. Gough, A. Rivera-Galletti, D.A. Cowan, D. Salas-de la Cruz, X. Hu, Protein and polysaccharide-based fiber materials generated from ionic liquids: A review, Molecules 25 (2020) 3362. https://doi.org/10.3390/molecules25153362

[47] M.G. Paredes, M.A. Mariño, R.A. Tapia, D.R. MacFarlane, K. Matuszek, D. Ruiz, M. Isaacs, P. Pavez, Protic ionic liquids based on anionic clusters ([Hmim][(HSO4)(H2SO4]x) with (x = 0, 1, and 2), to produce nanocellulose (CNC), J. Mol. Liq. 367 (2022) 120422. https://doi.org/10.1016/j.molliq.2022.120422

[48] A.V. Belesov, D.A. Lvova, D.I. Falev, I.I. Pikovskoi, A.V. Faleva, N.V. Ul'yanovskii, A.V. Ladesov, D.S. Kosyakov, Fractionation of arctic brown algae (fucus vesiculosus) biomass using 1-butyl-3-methylimidazolium-based ionic liquids, Molecules 28 (2023) 7596. https://doi.org/10.3390/molecules28227596

[49] H. Yang, J. Jiang, B. Zhang, W. Zhang, W. Xie, J. Li, Experimental study on pretreatment effects of [BMIM]HSO4/ethanol on the thermal behavior of cellulose, RSC Adv. 12 (2022) 10366-10373. https://doi.org/10.1039/D2RA00876A

[50] W. Li, Y. Wang, D. Li, J. Jiang, K. Li, K. Zhang, Q. An, S. Zhai, L. Wei, 1-Ethyl-3-methylimidazolium acetate ionic liquid as simple and efficient catalytic system for the oxidative depolymerization of alkali lignin, Int. J. Biol. Macromol. 183 (2021) 285-294. https://doi.org/10.1016/j.ijbiomac.2021.04.118

[51] L. Zhang, Y. Hu, X. Wang, A. Zhang, O.A. Fakayode, H. Ma, C. Zhou, Hybrid techniques of pre and assisted processing modify structural, physicochemical and functional characteristics of okra pectin: Controlled-temperature ultrasonic-assisted extraction from preparative dry powders and its field monitoring, Ultrason. Sonochem. 88 (2022) 106080. https://doi.org/10.1016/j.ultsonch.2022.106080

[52] M. Brehm, J. Radicke, M. Pulst, F. Shaabani, D. Sebastiani, J. Kressler, Dissolving cellulose in 1,2,3-triazolium- and imidazolium-based ionic liquids with aromatic anions, Molecules 25 (2020) 3539. https://doi.org/10.3390/molecules25153539

[53] X. Ma, X. Cheng, Y. Du, P. Tang, L. Chen, W. Chen, Z. Zheng, Pectins rich in RG-I extracted from watermelon peel: Physicochemical, structural, emulsifying, and antioxidant properties, Foods 13 (2024) 2338. https://doi.org/10.3390/foods13152338

[54] Q. Yuan, Y. He, P.Y. Xiang, Y.J. Huang, Z.W. Cao, S.W. Shen, L. Zhao, Q. Zhang, W. Qin, D.T. Wu, Influences of different drying methods on the structural characteristics and multiple bioactivities of polysaccharides from okra (Abelmoschus esculentus), Int. J. Biol. Macromol. 147 (2020) 1053-1063. https://doi.org/10.1016/j.ijbiomac.2019.10.073

[55] Y. Yu, Y. Wang, X. Liu, Y. Liu, L. Ji, Y. Zhou, L. Sun, Comparison of analytical methods for determining methylesterification and acetylation of pectin, Appl. Sci. 11 (2021) 4461. https://doi.org/10.3390/app11104461

[56] J. Tripathi, R. Ambolikar, S. Gupta, D. Jain, J. Bahadur, P.S. Variyar, Methylation of guar gum for improving mechanical and barrier properties of biodegradable packaging films, Sci. Rep. 9 (2019) 14505. https://doi.org/10.1038/s41598-019-50991-7

[57] A. Singh, S. Benjakul, T. Prodpran, P. Nuthong, Effect of psyllium (Plantago Ovata Forks) husk on characteristics, rheological and textural properties of threadfin bream surimi gel, Foods 10 (2021) 1181. https://doi.org/10.3390/foods10061181

[58] A. Kozioł, K. Środa-Pomianek, A. Górniak, A. Wikiera, K. Cyprych, M. Malik, Structural determination of pectins by spectroscopy methods, Coatings 12 (2022) 546. https://doi.org/10.3390/coatings12040546

[59] P.M. Wu, C.Y. Chung, Y.R. Chen, Y.H. Su, K.S. Chang-Liao, P.W. Chi, T. Paul, Y.J. Chen, Y.L. Chen, S.F. Wang, P. Badgujar, B.N. Chen, C.L. Cheng, M.K. Wu, Vibrational and electrochemical studies of pectin-a candidate towards environmental friendly lithium-ion battery development, PNAS Nexus 1 (2022) 127. https://doi.org/10.1093/pnasnexus/pgac127

[60] M. Szymańska-Chargot, P. Pękala, A. Siemińska-Kuczer, A. Zdunek, A determination of the composition and structure of the polysaccharides fractions isolated from apple cell wall based on FT-IR and FT-Raman spectra supported by PCA analysis, Food Hydrocoll. 150 (2024) 109688. https://doi.org/10.1016/j.foodhyd.2023.109688

[61] H. Zhang, Z. Li, Y. Wang, H. Zhang, A. Qayum, H. Meng, H. Fan, C. Zhu, Ethanol-graded fractionation reveals coordinated changes in composition, chain conformation, and rheology of hawthorn pectin, Int. J. Biol. Macromol. 343 (2026) 150316. https://doi.org/10.1016/j.ijbiomac.2026.150316

[62] W. Wang, X. Li, Z. Fang, J. Bi, Structural effect of polygalacturonase modified pectin on polyphenol enzymatic oxidation, Food Hydrocoll. 172 (2026) 112181. https://doi.org/10.1016/j.foodhyd.2025.112181

[63] S.T. Huang, C.H. Yang, P.J. Lin, C.Y. Su, C.C. Hua, Multiscale structural and rheological features of colloidal low-methoxyl pectin solutions and calcium-induced sol–gel transition, Phys. Chem. Chem. Phys. 23 (2021) 19269-19279. https://doi.org/10.1039/D1CP02778F

[64] Y. Xiao, Y. Yang, Y. Xu, L. Feng, M. Nie, L. Niu, C. Liu, C. Liu, D. Li, Z. Yu, Ultrasonic pretreatment and drying temperature-induced modifications of three pectin fractions affect the microstructure and textural properties of dried grapes, Food Chem. X 28 (2025) 102633. https://doi.org/10.1016/j.fochx.2025.102633

[65] S. Suttiruengwong, S. Konthong, S. Pivsa-Art, P. Plukchaihan, P. Meesuwan, M. Wanthong, N. Panpradist, R.A. Kurien, P. Pakawanit, P. Sriamornsak, Fabrication and characterization of porous pectin-based aerogels for drug delivery, Carbohydr. Polym. Technol. Appl. 7 (2024) 100499. https://doi.org/10.1016/j.carpta.2024.100499

[66] P. Perumal, P. Selvin, S. Selvasekarapandian, P. Sivaraj, K.P. Abhilash, V. Moniha, R. Manjula Devi, Plasticizer incorporated, novel eco-friendly bio-polymer based solid bio-membrane for electrochemical clean energy applications, Polym. Degrad. Stab. 159 (2019) 43-53. https://doi.org/10.1016/j.polymdegradstab.2018.11.013

[67] Y. Zhang, J. Qi, W. Zeng, Y. Huang, X. Yang, Properties of dietary fiber from citrus obtained through alkaline hydrogen peroxide treatment and homogenization treatment, Food Chem. 311 (2020) 125873. https://doi.org/10.1016/j.foodchem.2019.125873

[68] D. Zannini, G. Dal Poggetto, M. Malinconico, G. Santagata, B. Immirzi, Citrus pomace biomass as a source of pectin and lignocellulose fibers: From waste to upgraded biocomposites for mulching applications, Polymers 13 (2021) 1280. https://doi.org/10.3390/polym13081280

[69] C. Wang, Z. Zhu, C. Sun, L. Mei, W. Xue, X. Chen, X. Du, Structural disorganization and orientation of high-amylose maize starch with improved oil absorption capacity: Effects of water-ionic liquid ratios, Int. J. Biol. Macromol. 285 (2025) 138397. https://doi.org/10.1016/j.ijbiomac.2024.138397

[70] M. Tsirigotis-Maniecka, E. Górska, A. Mazurek-Hołys, I. Pawlaczyk-Graja, Unlocking the potential of food waste: A review of multifunctional pectins, Polymers 16 (2024) 2670. https://doi.org/10.3390/polym16182670

[71] S. Chatterjee, P.C. Hui, Review of applications and future prospects of stimuli-responsive hydrogel based on thermo-responsive biopolymers in drug delivery systems, Polymers 13 (2021) 2086. https://doi.org/10.3390/polym13132086

[72] M. Duggal, D.P. Singh, S. Singh, S. Khubber, M. Garg, M. Krishania, Microwave-assisted acid extraction of high-methoxyl kinnow (Citrus reticulata) peels pectin: Process, techno-functionality, characterization and life cycle assessment, Food Chem. Mol. Sci. 9 (2024) 100213. https://doi.org/10.1016/j.fochms.2024.100213

[73] S. Liu, Y. Yu, K. Ni, T. Liu, M. Gu, Y. Wu, G. Du, X. Ran, Construction of a novel electrochemical sensor based on biomass material nanocellulose and its detection of acetaminophen, RSC Adv. 12 (2022) 27736-27745. https://doi.org/10.1039/D2RA04125A

[74] J. Wang, C. Zhao, P. Li, L. Wang, S. Li, Structural characteristics and multiple bioactivities of volvariella volvacea polysaccharide extracts: The role of extractive solvents, Foods 12 (2023) 4357. https://doi.org/10.3390/foods12234357

[75] B. Kocaaga, T. Inan, N.I. Yasar, C.E. Yalcin, F.A. Sungur, O. Kurkcuoglu, A. Demiroz, H. Komurcu, O. Kizilkilic, S.Y. Aydin, O. Aydin Ulgen, F.S. Güner, H. Arslan, Innovative use of an injectable, self-healing drug-loaded pectin-based hydrogel for micro- and supermicro-vascular anastomoses, Biomacromolecules 25 (2024) 3959-3975. https://doi.org/10.1021/acs.biomac.4c00102

[76] S. Parajuli, M.J. Hasan, E.E. Ureña-Benavides, Effect of the interactions between oppositely charged cellulose nanocrystals (CNCS) and chitin nanocrystals (CHNCS) on

the enhanced stability of soybean oil-in-water emulsions, Materials 15 (2022) 6673. https://doi.org/10.3390/ma15196673

[77] Y. Jiang, S. Zhao, F. Wang, X. Zhang, Z. Su, Highly stretchable double network ionogels for monitoring physiological signals and detecting sign language, Biosensors 14 (2024) 227. https://doi.org/10.3390/bios14050227

Conflicts of interest

The authors declared that they have no conflicts of interest to this work.

Hao Zhang: hao.zhang@doct.uliege.be

Huiyao Zhang: 2465727776@qq.com

Jiachen Li: 123101485@umail.ucc.ie

Yugui Wang: Yugui.Wang@uky.edu

Hongbing Fan (Hongbing.Fan@uky.edu)

Christophe Blecker (christophe.blecker@uliege.be)

Chuanhe Zhu: chhzhu@sdau.edu.cn